Industrial Crops & Products 251 (2026) 124180

Contents lists available at ScienceDirect

Industrial Crops & Products

journal homepage: www.elsevier.com/locate/indcrop

Metal-organic frameworks (MOF)-mediated improvement of cotton germination and early seedling resilience under salinity stress through explainable machine learning and non-destructive terahertz time-domain spectroscopy (THz-TDS)

Muhammad Tanveer Altaf [a], Kholoud Elmabruk [b], Salma Naimatullah Soomro [c], Sabeen Rehman Soomro [c], Tülay Aksoy [d], Kağan Murat Pürlü [b], Seyid Amjad Ali [e], Emre Biçer [f], Sabit Horoz [d], Waqas Liaqat [a], Kağan Kökten [g], Muhammad Aasim [h,*,1]

[a] Department of Field Crops, Faculty of Agriculture, Recep Tayyip Erdoğan University, Pazar, Rize, Turkey
[b] Faculty of Engineering and Natural Sciences, Electrical and Electronics Engineering Department, Sivas University of Science and Technology, Sivas, Turkey
[c] Faculty of Agricultural Sciences and Technology, Sivas University of Science and Technology, Sivas, Turkey
[d] Department of Engineering Fundamental Sciences, Faculty of Engineering, Sivas University of Science and Technology, Sivas, Turkey
[e] Department of Information Systems and Technologies, Bilkent University, Ankara, Turkey
[f] Department of Chemistry, Faculty of Sciences, Ankara University, Ankara, Turkey
[g] Department of Field Crops, Faculty of Agricultural Sciences and Technology, Sivas University of Science and Technology, Sivas, Turkey
[h] Department of Precision Agriculture and Agricultural Robotics, Faculty of Agricultural Sciences and Technology, Sivas University of Science and Technology, Sivas, Turkey

A R T I C L E I N F O

Keywords:
Cotton
Metal-organic framework
Multi-output regression
Terahertz time-domain spectroscopy
Explainable machine learning

A B S T R A C T

Cobalt-based metal-organic framework (Co-MOF) and nickel-cobalt bimetallic MOF (Ni-Co-MOF) systems were evaluated for their effects on cotton germination under saline conditions induced through NaCl seed priming treatments. Temporal germination dynamics, germination-related indices, explainable machine learning (ML), and terahertz time domain spectroscopy (THz-TDS) were integrated to characterize treatment-associated germination and THz responses. The results demonstrated clear treatment-dependent differences in germination initiation, progression, synchronization, and cumulative germination behavior. Co-MOF at 50 mg/L produced the strongest early germination responses, whereas Ni-Co-MOF at 50 mg/L achieved the highest cumulative germination (91.0%). A 4 h priming duration produced the most coordinated germination pattern under saline conditions. The random forest-based multi-output regression framework showed variable predictive performance among germination indices, with an average R^2 of 0.372 and a maximum R^2 of 0.507 for mean germination rate. Feature importance analysis further revealed that intermediate germination stages contributed most strongly to predictive performance. THz-TDS analysis revealed clear treatment-associated differences in time-domain attenuation and frequency-dependent absorption profiles within cotton leaf tissues. Stronger attenuation and absorption responses observed under specific MOF treatments indicated treatment-associated variation in hydration-associated dielectric behavior. Compared with 100 mM NaCl reference treatment without MOF supplementation,selected MOF treatments exhibited higher cumulative germination and distinct THz responses. The integration of MOF treatments, THz-TDS, and explainable ML provided a combined analytical approach for characterizing early germination patterns and leaf THz responses under controlled saline conditions. However, However, there is a need of further biochemical, physiological, ion-homeostasis, and plant growth assessments are needed to clarify the underlying mechanism.

* Corresponding author.
E-mail address: maasim@sivas.edu.tr (M. Aasim).
1 ORCID: 0000-0002-8524-9029

https://doi.org/10.1016/j.indcrop.2026.124180
Received 31 May 2026; Received in revised form 8 August 2026; Accepted 14 August 2026
Available online 20 August 2026

1. Introduction

Salinity stress poses serious risks to sustainable crop production under changing climatic conditions and is regarded as one of the most severe abiotic constraints limiting agricultural productivity globally (Okumuş et al. 2024). Through osmotic stress, ionic toxicity, nutrient imbalance, oxidative damage, and disruption of metabolic activity, excessive salt buildup in soil negatively impacts plant growth and development, ultimately lowering crop establishment and productivity (Yousef et al., 2020). Despite being more tolerant than some glycophytic crops, cotton (*Gossypium hirustum* L.) is still extremely susceptible to salinity stress during germination and the early stages of seedling establishment (Bakhsh et al., 2015). Improving germination performance and early seedling establishment under salişne environments remains an important challenge for sustainable cotton production systems, since successful germination is a crucial factor in crop establishment and subsequent productivity. Therefore, compared to final germination percentage alone, temporal germination dynamics and germination-associated physiological indices offer a more thorough understanding of stress-associated responses (Aasim et al., 2024; Altaf et al., 2026).

To improve germination and early seedling establishment, seed priming with functional nanomaterials, including metal-oxide, biostimulants, polymers, and other state-of-the-art compounds. However, Metal-organic frameworks (MOFs) differ structurally from conventional nanomaterials because they are porous, crystalline materials composed of organic ligands and metal ions, with a wide array of topologies and functionalities (Muthalagu and Natarajan, 2025). Among advanced nanomaterials, MOFs have attracted increasing attention for their tunable porous structures, high surface areas, exceptional sorption capacities, and functional versatility, which may support stress adaptation and physiological stabilization under adverse environmental conditions (Rojas et al., 2022). Compared with conventional functional nanomaterials, MOFs may provide controlled physicochemical interactions through their tunable metal-ligand compositions and porous structure, which also support their application as controlled -delivery platforms. MOF-based delivery has been demonstrated in different disciplines (Nie et al., 2020), while agricultural research has primarily focused on nutrient, agrochemical, and plant growth responses (Mahmoud and Abdelhameed, 2025; Masood et al., 2025; Muthalagu and Natarajan, 2025). Recent studies have also demonstrated that the effects of MOFs on plants can vary with their metal composition (Elkelish et al., 2026; Liu et al., 2026) as reported for Ni, Co, Cr, and Cu-based MOFs in faba bean (Mahmoud and Abdelhameed, 2025). However, limited information is available regarding the effects of MOF-mediated systems on temporal germination physiology and salinity adaptation in cotton, especially under controlled in vitro conditions. The biological contribution of this study is the integrated evaluation of Co-MOF and Ni-Co-MOF effects on cotton germination under salinity conditions to compare mono- and bimetallic frameworks that may produce concentration-dependent plant responses (Elkelish et al., 2026; Liu et al., 2026). Salinity stress induces physiological, biochemical, and structural changes in plants, particularly during early developmental stages. Accurate characterization of these responses is therefore essential for understanding stress adaptation mechanisms and improving stress-resilient cropping systems. Under in vitro conditions, plants remain continuously exposed to controlled stress conditions for a prolonged time, providing suitable material for detailed physiological characterization. Conventional approaches for physiological characterization often rely on destructive sampling methods and labor-intensive analyses, limiting continuous monitoring of dynamic stress responses (Wu et al., 2024; Alibeigloo et al., 2025). Therefore, non-destructive analytical approaches capable of tracking physiological and structural responses in real time are receiving increasing attention (Ginzburg et al., 2024; Muhammad et al., 2025). Terahertz Time-domain Spectroscopy (THz-TDS) is a non-destructive spectroscopic method for detecting hydration-sensitive dielectric changes in biological tissues (Alibeigloo et al., 2025). THz radiation is highly sensitive to water status, hydrogen-bond-associated molecular dynamics, dielectric properties, and structural organization within plant tissues (Castro-Camus et al., 2025; You et al., 2025).

Because ML approaches can effectively model complex stress-response dynamics, multidimensional physiological variability, and nonlinear biological relationships, they are increasingly being applied in agricultural and plant stress research (Aasim et al., 2026; Saini et al., 2026), particularly alongside recent advances in spectroscopic plant phenotyping techniques (Zarbakhsh et al., 2025). Conventional statistical approaches often show limitations in characterizing the nonlinear and temporally dynamic nature of germination-associated stress responses. Random Forest (RF)-based models are considered robust analytical tools because of their ability to capture nonlinear relationships, reduce overfitting, and identify biologically informative variables within complex biological datasets (Altaf et al., 2026). In addition, explainable artificial intelligence (AI) approaches, such as feature importance analysis (Zhu et al., 2024), can identify the temporal variables most strongly associated with predictive performance, thereby supporting biological interpretation. However, limited information is available regarding the combined application of temporal germination dynamics, explainable ML, and THz-TDS-based physiological characterization for evaluating MOF-associated salinity adaptation in cotton. Therefore, the current study sought to: (i) assess how MOF-associated salinity treatments affected cotton's temporal germination dynamics and germination-related physiological indices; (ii) use RF-based multi-output regression modelling to characterize predictive relationships among germination-associated traits; (iii) use feature importance analysis to identify physiologically informative germination stages; and (iv) use THz-TDS to examine treatment-associated dielectric and hydration-related physiological responses. Thus, the novelty of the present study lies not in a new MOF synthesis route or a new ML algorithm; rather, it presents the biological implications of multiple MOF treatments by integrating temporal germination profiling, explainable RF modeling, and non-destructive THz-TDS phenotyping for guiding targeted physiological validation.

2. Material and methodology

2.1. Preparation of metal-organic frameworks (MOFs)

The Co-MOF was synthesized hydrothermally using cobalt (II) acetate [$Co(CH_3COO)_2$] as the metal precursor and and pyrazine−2–3-dicarbozylic acid (PyDCA, ≥98% purity) as the organic linker. Deionized distilled water was used as the solvent in all experiments, and all reagents were used without any further purification or processing. $Co(CH_3COO)_2$ was dissolved in 50 ML of deionized water under magnetic stirring at room temperature, followed by the addition of PyDCA and continuous stirring for 30 min to promote metal-ligand coordination. The resulting homogeneous solution was transferred into a Teflon-lined stainless-steel autoclave and heated at 120 C for 25 h under static hydrothermal conditions. After natural cooling to room temperature, the synthesized product was collected by vacuum filtration, washed thrice with deionized water to remove residual reactants and soluble impurities, and dried at 60 C for 12 h to obtain Co-MOF powder (Özdemir et al., 2026). The Ni-Co bimetallic MOF was synthesized following the same hydrothermal procedure, except that an equimolar amount of $Co(CH_3COO)_2$] and nickel(II) acetate [$Ni(CH_3COO)_2$] was used as co-metal precursors while maintaining the same total metal-to-linker molar ratio. The mixed-metal precursor solution was reacted with PyCDA under identical hydrothermal conditions to obtain Ni-Co-MOF, which was subsequently washed and dried using the same procedure described for Co-MOF.

2.2. Experimental setup

Cotton (*Gossypium hirsutum* L.) cultivar STN−468 was used as the plant material in the present study. Healthy and uniform seeds were initially surface sterilized using 0.1% mercuric chloride ($HgCl_2$) solution for 15 min to eliminate potential microbial contamination. Following sterilization, the seeds were thoroughly rinsed three times with sterile distilled water to remove residual sterilizing agent and minimize possible toxic effects on subsequent germination. The experiment followed a factorial design with three replications, containing 6 seeds per jar. The combinations used in this study comprised two concentrations of sodium chloride (NaCl) solutions (25, 50, and 100 mM), three priming time (2, 4, and 8 h), two MOF types (Co-MOF and Ni-Co-MOF), and two concentrations (50 or 100 mg/L). The combinations used in this study are presented in Table 1. The 100 mM NaCl treatment without MOFs was used as a salinity reference. Both MOFs were incorporated into Murashige and Skoog (MS) culture medium prepared as standard medium (4.4 g/L MS, 30 g/L sucrose, 6.5 g/L agar, and pH ≈ 5.8). These concentrations were selected as exploratory working levels for comparing dose-dependent MOF responses under in vitro conditions, rather than the isolated effects of their chemical components. The cultured vessels were maintained under controlled in vitro growth conditions at 25 ± 2 °C with a 16 h light/8 h dark photoperiod and relative humidity of approximately 60–70%. Seeds treated with 100 mM NaCl and cultured without MOF supplementation were used as the reference treatment for comparative evaluation of germination dynamics, machine learning (ML) modeling, and THz-TDS-associated dielectric responses under saline conditions.

2.3. Cumulative germination analysis

The germination data were recorded daily for 12 consecutive days at 24 h intervals to analyze the cumulative germination percentage and germination indices. Cumulative germination percentage was computed for each treatment, followed by generating trajectories to assess treatment-associated variation in germination initiation, progression, synchronization, and stabilization behavior. All experiments were performed in triplicate, and the results are presented as mean cumulative germination percentages with standard error (SE) represented by vertical error bars. The trajectories were used to present the treatment-associated temporal patterns and interpreted as numerical trends.

2.4. GerminaR-based germination index analysis

Germination indices were calculated from the daily germination count data using the GerminaR package in R. The evaluated indices included germination percentage (GRP), mean germination time (MGT), mean germination rate (MGR), germination speed percentage (GSP), uncertainty index (UNC), synchronization index (SYN), vigor index (VGT), standard deviation of germination time (SDG), and coefficient of velocity of germination (CVG).

$$GRP = \frac{\sum_{i=1}^{k} n_i}{N} \times 100 \tag{1}$$

where n_i is the number of seeds germinated in the i^{th} time; N represents the total number of seeds in each experimental unit; k refers to the last day of germination evaluation.

$$MGT = \frac{\sum_{i=1}^{k} n_i t_i}{\sum_{i=1}^{k} n_i} \tag{2}$$

where n_i represents the number of seeds germinated at time t_i, t_i is the time from the beginning of the experiment to the i^{th} observation, and $\sum n_i$ represents the total number of seeds that are germinated.

$$MGR = \frac{\sum_{i=1}^{k} n_i}{\sum_{i=1}^{k} n_i t_i} \tag{3}$$

where n_i represents the number of seeds germinated at the time t_i, t_i denotes the corresponding germination time (days or hours), and $\sum n_i$ represents the total number of germinated seeds.

$$GSP = \frac{\sum_{i=1}^{k} G_i}{\sum_{i=1}^{k} G_i X_i} \times 100 \tag{4}$$

G_i is the number of seeds germinated in the i^{th} time, and X_i represents the number of days from sowing.

Table 1
Germination indices of in vitro cotton seedlings under MOF-NaCl treatments.

MOF	Time	Conc	NaCl	GRP	MGT	MGR	GSP	UNC	SYN	VGT	SDG	CVG
Ni	2	25	25	83.33	3.80	0.263	26.31	1.922	0.100	6.20	2.490	65.52
Ni	4	25	25	50.00	3.00	0.333	33.33	0.918	0.333	3.00	1.732	57.73
Ni	8	25	25	50.00	4.00	0.250	25.00	1.585	0.000	9.00	3.000	75.00
Ni	2	50	50	33.33	2.00	0.500	50.00	1.000	0.000	2.00	1.414	70.71
Ni	4	50	50	83.33	4.40	0.227	22.72	1.922	0.100	10.80	3.286	74.68
Ni	8	50	50	66.66	2.50	0.400	40.00	1.000	0.333	3.00	1.732	69.28
C	2	0	100	66.66	4.00	0.250	25.00	1.500	0.167	6.00	2.449	61.23
C	4	0	100	66.66	3.25	0.308	30.76	1.500	0.167	8.25	2.872	88.37
C	8	0	100	50.00	4.33	0.231	23.07	1.585	0.000	10.33	3.215	74.18
Ni-Co	2	25	25	50.00	4.33	0.231	23.07	1.585	0.000	17.33	4.163	96.07
Ni-Co	4	25	25	66.66	2.00	0.500	50.00	1.500	0.167	2.00	1.414	70.71
Ni-Co	8	25	25	33.33	1.50	0.667	66.66	1.000	0.000	0.50	0.707	47.14
Ni-Co	2	50	50	50.00	2.66	0.375	37.50	1.585	0.000	9.33	3.055	114.56
Ni-Co	4	50	50	100.0	2.83	0.353	35.29	1.918	0.133	9.76	3.125	110.30
Ni-Co	8	50	50	66.67	2.75	0.364	36.36	2.000	0.000	7.58	2.754	100.13
C	2	0	100	83.33	4.00	0.250	25.00	1.922	0.100	9.50	3.082	77.05
C	4	0	100	33.33	3.50	0.286	28.57	1.000	0.000	12.50	3.536	101.01
C	8	0	100	50.00	3.00	0.333	33.33	1.585	0.000	7.00	2.646	88.19

MOF: metal-organic frameworks, Ni: Nickel, Co: Cobalt, C: control, GRP: germination percentage, MGT: mean germination time, MGR: mean germination rate, GSP: germination speed percentage, UNC: uncertainty index, SYN: synchronization index, VGT: vigor index, SDG: standard deviation of germination time, and CVG: coefficient of velocity of germination

$$UNC = -\sum_{i=1}^{k} f_i \log_2 f_i \ with \ f_i = \frac{n_i}{\sum_{i=1}^{k} n_i} \quad (5)$$

$$SYN = \frac{\sum_{i=1}^{k} C_{n_i,2}}{C_{\sum n_i,2}} \ with \ C_{n_i,2} = \frac{n_i(n_i - 1)}{2} \quad (6)$$

$$VGT = \frac{\sum_{i=1}^{k} n_i (t_i - \bar{t})^2}{\sum_{i=1}^{k} n_i - 1} \quad (7)$$

where n_i represents the number of seeds germinated at a time t_i, t_i denotes the germination time (days or hours), $\bar{t}$ is the Mean Germination Time, and $\sum n_i$ represents the total number of germinated seeds.

$$SDG = \sqrt{VGT} = \sqrt{\frac{\sum_{i=1}^{k} n_i (t_i - \bar{t})^2}{\sum_{i=1}^{k} n_i - 1}} \quad (8)$$

where n_i represents the number of seeds germinated at time t_i, t_i denotes the germination time (days or hours), $\bar{t}$ represents the mean germination time, k is the final germination observation time, and $\sum n_i$ represents the total number of germinated seeds.

$$CVG = \left(\frac{\sqrt{VGT}}{MGT}\right) \times 100 \quad (9)$$

where VGT represents the variance of germination time, and MGT denotes the mean germination time.

2.5. Random forest-based multiple output regression analysis

A multi-output regression framework was employed to simultaneously predict multiple germination-associated traits from a common set of input variables (Wang et al., 2024). This approach captures the interrelationship among target traits while reducing redundant computation compared with independent single-output models (Tsoumakas and Vlahavas, 2007; Borchani et al., 2015). In the present study, Random Forest (RF) regression (Breiman, 2001) was used as the prediction model because of its ability to model nonlinear relationships and complex physiological interactions without strict distributional assumptions (Hoffman et al., 2021). Each tree in the ensemble model was trained using bootstrap samples, and predictions for all output traits were obtained by averaging across trees. In this study, the RF model was tuned using leave-one-out cross-validation (LOOCV) because of the limited number of experimental datasets. This validation strategy offers the complete utilization of datasets, with each experimental unit undergoing testing and training. During each LOOCV iteration, one observation was used for validation while remaining observations were used for model training. Although LOOCV is an efficient strategy for validation of limited datasets, it does not replace independent external validation and hence should be interpreted as an internal estimate of model generalization. The performance of the model was computed with four different performance metrics, namely: Coefficient of Determination (R^2), Root Mean Square Error (RMSE), Mean Absolute Error (MAE), Relative Root Mean Square Error (RRMSE), and Symmetric Mean Absolute Percentage Error (SMAPE). To provide additional context for model performance, the RF model was compared with simpler regression approaches, including Linear Regression, Ridge Regression, Partial Least Squares (PLS) Regression, and a Dummy baseline model. All comparison models were evaluated using the same LOOCV procedure and performance metrics. allowing a consistent assessment of the suitability of Random Forest for modeling nonlinear germination responses.

$$R^2 = 1 - \frac{\sum_{i=1}^{n} (Y_i - \widehat{Y}_i)^2}{\sum_{i=1}^{n} (Y_i - \overline{Y})^2} \quad (10)$$

$$RMSE = \sqrt{\frac{1}{n} \sum_{i=1}^{n} (Y_i - \widehat{Y}_i)^2} \quad (11)$$

$$MAE = \frac{1}{n} \sum_{i=1}^{n} |Y_i - \widehat{Y}_i| \quad (12)$$

$$RRMSE = \sum_{i=1}^{n} \frac{\sqrt{\frac{1}{n} \sum_{i=1}^{n} (Y_i - \widehat{Y}_i)^2}}{\frac{1}{n} \sum_{i=1}^{n} Y_i} \times 100 \quad (13)$$

$$SMAPE = \frac{1}{n} \sum_{i=1}^{n} \frac{|Y_i - \widehat{Y}_i|}{0.5(|Y_i| + |\widehat{Y}_i|)} \times 100 \quad (14)$$

where Y_i represents the actual value, $\widehat{Y}_i$ represents the predicted value, and n denotes the total number of observations.

Hyperparameter tuning was done for the number of trees and the maximum depth, and the best model was selected by minimizing the sum of root mean square errors (RMSEs) for all traits (Eq. 8). This criterion ensures balanced accuracy so that improving one trait does not compromise others.

$$\theta^* = \ argmin_\theta \sum_{j=1}^{m} RMSE_j(\theta)$$

where θ denotes the hyperparameters of the Random Forest model.

2.6. Feature importance analysis

To identify the most influential predictors governing cotton germination behaviour under MOF-associated salinity treatments, feature importance was evaluated using permutation importance based on the RF-based multi-output regression framework. Unlike impurity-based importance measures, permutation importance estimates the contribution of each predictor by measuring the decrease in model performance after randomly permuting the values of that predictor while leaving all other variables unchanged. The evaluated input variables included MOF type, NaCl level, priming duration, MOF concentration, and daily germination observations (D_0–D_1). Permutation importance was evaluated for each germination trait using held-out observations under the LOOCV framework, normalized within each output, and subsequently summarized as the mean ± SE across all germination traits to obtain an overall importance profile. Although the evaluated indices were derived from daily germination counts, they represent distinct dimensions of germination behavior. Therefore, feature importance analysis was used as a temporal-attribution approach to identify the specific days exerting the greatest influence on the overall germination profile.

2.7. Dielectric properties characterization

The dielectric behavior of cotton leaf tissues was investigated using Terahertz Time-Domain Spectroscopy (THz-TDS). THz-TDS is a rapid, non-contact, and non-destructive technique highly sensitive to hydration-associated dielectric properties and structural heterogeneity in biological tissues. The technique enables rapid characterization of treatment-associated spectral and dielectric patterns in plant tissues under abiotic stress conditions without destructive sampling. Fig. 1 presents the schematic illustration of the THz-TDS experimental configuration used for leaf measurements using a commercial TeraFlash Pro system (TOPTICA Photonics, Germany) operated in transmission

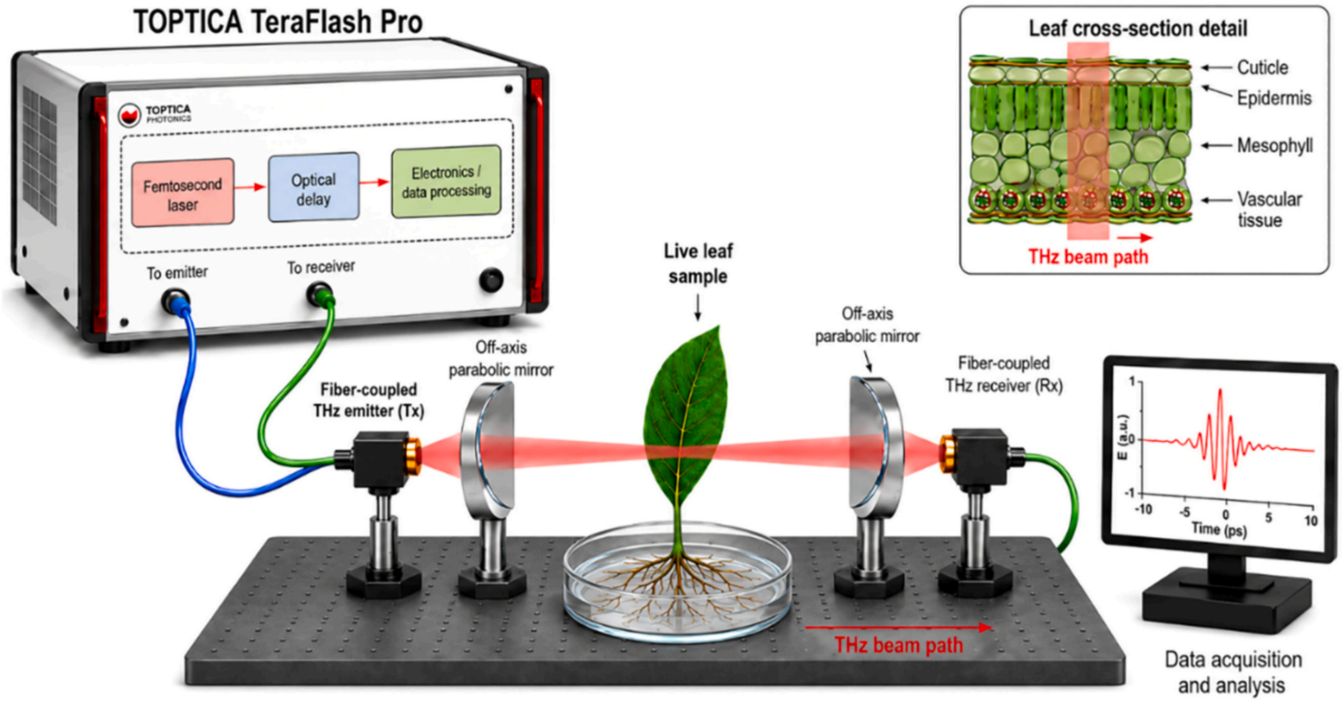

Fig. 1. Schematic diagram of the THz-TDS measurement setup.

mode. The transmitted THz electric field was recorded in the time domain through temporal delay-line scanning. Reference THz waveforms were first recorded in air, followed by measurements of a cotton leaf sample under identical experimental conditions for comparison of treatment-associated dielectric responses. The recorded time-domain electric field, E(t), was converted into the frequency domain using the Fourier transform (Purlu et al., 2026).

$$E(t) \xrightarrow{FT} \frac{1}{\sqrt{2\pi}} \int_{-\infty}^{\infty} E(t)e^{-i\omega t}\mathrm{d}t = E(\omega) \tag{15}$$

The resulting frequency-domain signal is complex and can be represented in terms of its amplitude and phase as (Purlu et al., 2026).

$$E(\omega) = A(\omega)e^{i\phi(\omega)} \tag{16}$$

where $A(\omega)$ and $\phi(\omega)$ denote the spectral amplitude and phase, respectively. Because THz-TDS directly provides both amplitude and phase information, the optical and dielectric parameters of the leaf samples can be extracted without requiring the Kramers–Kronig transformation.

The absorption coefficient is obtained from the amplitude ratio of the sample and reference signals as [1]

$$\alpha(\omega) = -\frac{2}{d}\ln\left(\frac{A_{sample}}{A_{ref}}\right) \tag{17}$$

where $A_{sam}(\omega)$ and A_{ref} (ω) are the amplitudes of the transmitted THz spectra measured with and without the leaf sample, respectively. The negative sign ensures a positive absorption coefficient when the transmitted amplitude decreases after passing through the leaf tissue.

Higher TDZ absorption and damping responses were interpreted as indicators of changes in tissue hydration dynamics, dielectric organization, and stress-associated physiological adaptation in cotton leaf tissues. For data processing, the acquired reference and sample THz waveforms were transformed into frequency-domain spectra using Fast Fourier Transform (FFT) analysis in MATLAB. Identical signal-processing parameters were applied to all spectra. The effective thickness of each leaf specimen was determined from repeated measurements at multiple locations on the leaf surface, and the average value was used for dielectric analysis. The mean thickness of each leaf was used as d in the absorption-coefficient calculation, and thickness variability was reported as ± standard deviation. Each sample spectrum was normalized to the corresponding air-reference spectrum recorded under identical conditions before averaging. The analysis enabled the extraction of the frequency-dependent refractive index, absorption coefficient, relative permittivity, and dielectric loss tangent across the investigated THz frequency range.

3. Results

3.1. Characterization of MOF

The XRD patterns of both MOFs are presented in Fig. 2, which revealed numerous sharp and well-resolved diffraction peaks across the

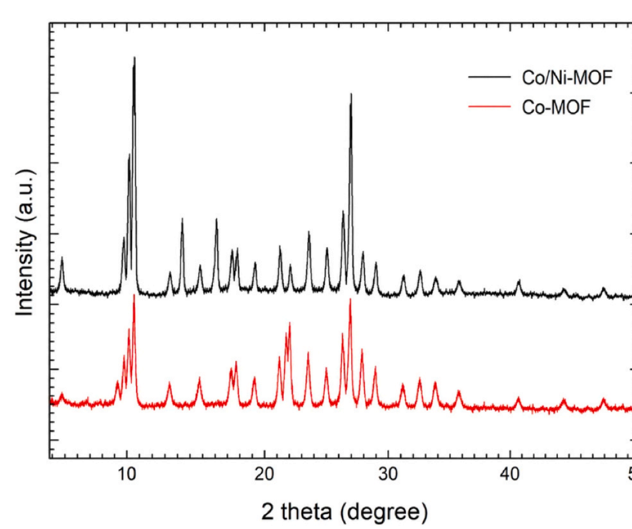

Fig. 2. Powder X-ray diffraction (XRD) patterns of Co-MOF (black) and Co/Ni-MOF (red).

2θ range of 5–50°, indicating information about the crystal structure and crystallinity of pyrazine−2,3-dicarboxylic acid (H_2pzdc)-based products. Co-MOF showed closely spaced reflections at $2\theta \approx 9$–11°, medium-intensity peaks between 13° and 24°, and a strong reflection near 6–27°. Whereas the Ni-Co-MOF diffractogram closely overlapped with that of Co-MOF in terms of peak positions, indicating preservation of a similar crystalline framework. No additional reflections attributable to separate crystalline phases were observed.

3.2. Time-series-based cumulative germination analysis

The cumulative germination profiles showed numerical treatment-associated differences in germination progression under both MOF treatments (Fig. 3). Supplementation of 50 mg/L Co-MOF showed earlier germination initiation and a higher mean cumulative germination during the intermediate developmental stage (Fig. 3a). Whereas a slower early germination response followed by a gradual late-stage increase in cumulative germination (75.0%) was recorded for 25 mg/L Co-MOF. In contrast, relatively delayed germination with reduced cumulative germination (54.0%) was recorded for the reference treatment. Similar observations were also recorded for Ni-Co-MOF, with a maximum cumulative germination of 91.0% recorded for 50 mg/L. Clear salinity- and duration-associated shifts in temporal germination response were also observed under both MOF systems (Fig. 3b,c). The 50 mM NaCl-associated treatments showed relatively stable and sustained progression relative to the 100 mM NaCl reference condition, with a higher mean germination trajectory (Fig. 3b). Priming duration was associated with numerical differences in germination coordination, with the 4 h priming treatment showed the most synchronized and sustained mean trajectory (Fig. 3c). Temporal germination trajectories further display clear differences in germination initiation, progression, and saturation phases between Co-MOF and Ni-Co-MOF systems, with Ni-Co-MOF exhibiting stronger enhancement of germination kinetics under saline environmental conditions. These findings overall indicate treatment–associated regulation of temporal germination dynamics during salt stress exposure in cotton.

3.3. Multi-output regression analysis

The results of computed germination indices (Table 1) were subjected to RF-based multioutput regression analysis to evaluate the relationships among germination-associated traits. Overall, the multiple-

Table 2
Predictive performance metrics of the Random Forest-based multi-output regression model for germination-related traits under MOF-mediated salinity stress environmental conditions.

Trait	R^2	RMSE	MAE	RRMSE	SMAPE
GRP	0.445	10.862	9.045	15.800	13.490
MGT	0.382	0.579	0.423	13.030	10.040
MGR	0.507	0.033	0.025	14.200	10.210
GSP	0.485	3.375	2.380	14.520	9.710
UNC	0.361	0.297	0.252	13.320	11.710
SYN	0.373	0.048	0.038	106.030	139.180
VGT	0.418	2.519	2.099	26.140	23.370
SDG	0.465	0.409	0.348	13.400	11.770
CVG	−0.084	9.881	8.679	14.300	12.570

GRP: germination percentage, MGT: mean germination time, MGR: mean germination rate, GSP: germination speed percentage, UNC: uncertainty index, SYN: synchronization index, VGT: vigor index, SDG: standard deviation of germination time, CVG: coefficient of velocity of germination, R^2: Coefficient of Determination, RMSE: Root Mean Square Error, MAE: Mean Absolute Error, RRMSE: Relative Root Mean Square Error, and SMAPE: Symmetric Mean Absolute Percentage Error

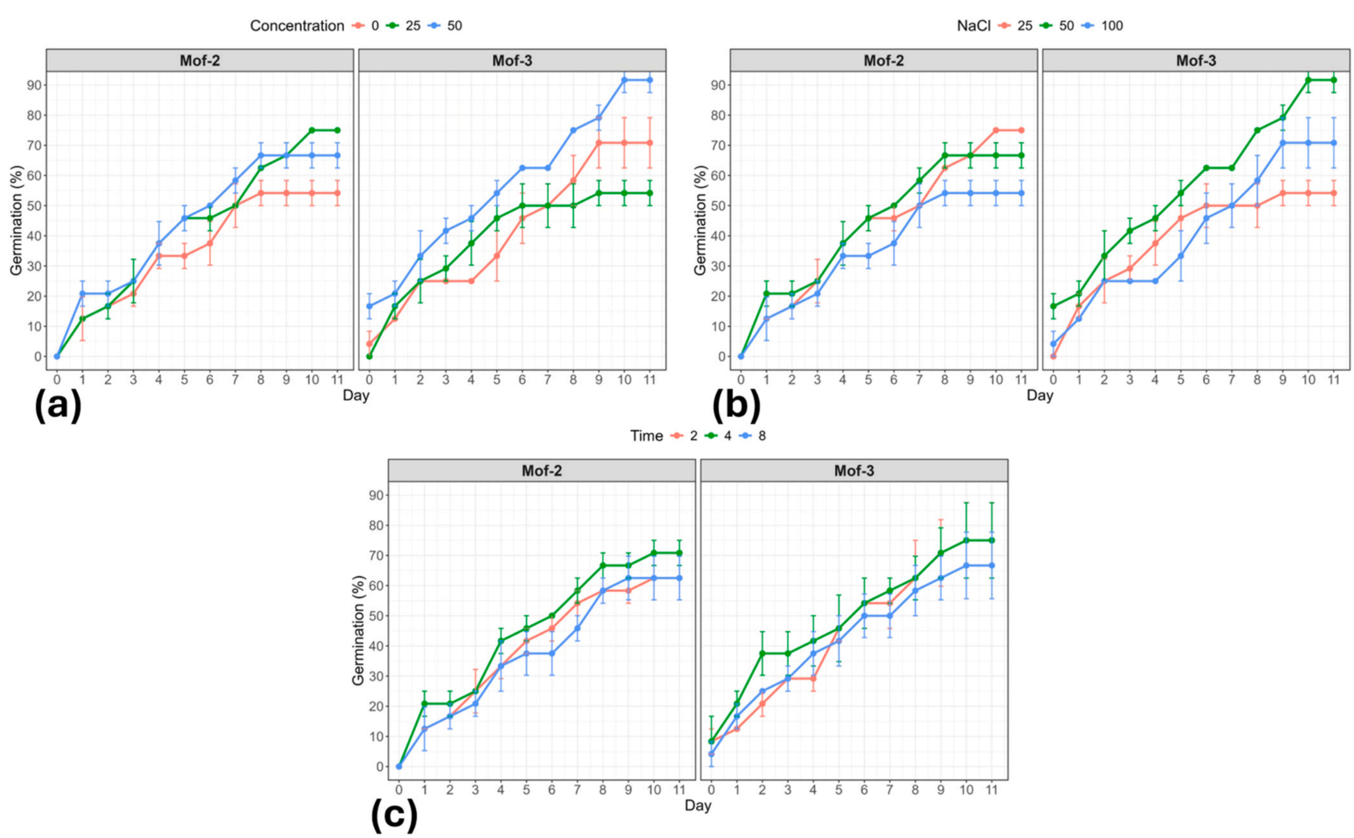

Fig. 3. Time series-based cumulative germination performance of MOF and NaCl (a) MOF concentration, (b) NaCl concentration, and (c) priming timing; values are means ± SE of three biological replicates and curves show descriptive temporal patterns among treatments.

output regression system yielded an average R^2 score of 0.372 (Table 2). The highest predictive performance was with an R^2 score of 0.507, accompanied by low RMSE (0.033), RRMSE (14.20%), and a SMAPE score of 10.21%. Likewise, GSP and SDG metrics also exhibited moderate R^2 scores and were recorded as 0.485 and 0.465, respectively. The error metrics for both germination traits were also low. Whereas GRP and BGT also exhibited moderate predictability with an R^2 score of 0.445 and 0.418, respectively; however, their error metric scores were relatively higher than GSP and SDG. Traits associated with germination timing, synchronization, and uncertainty, including MGT ($R^2 = 0.382$), UNC ($R^2 = 0.361$), and SYN ($R^2 = 0.373$), exhibited relatively lower predictive performance. In particular, SYN displayed exceptionally high relative error values (RRMSE = 106.03% and SMAPE = 139.18%), indicating comparatively limited learnability of this trait, potentially due to its narrow distribution and biological vari*ability. CVG also showed limited predictive performance, with a negative R^2 value ($R^2 = -0.084$). The RF-based multi-output framework identified trait-dependent nonlinear patterns, with comparatively better predictive performance for MGR, GSP, SDG, and GRP. The experimental observations and predicted scores of all germination indices are presented in Fig. 4. Comparative analysis of RF model with other models demonstrated superior capability for capturing the nonlinear relationships among germination-related variables. In addition, a Y-permutation test confirmed that the observed predictive performance was significantly greater than expected by chance ($p < 0.01$), supporting the presence of meaningful biological relationships within the dataset.

3.4. Feature importance analysis

Permutation feature importance analysis was performed to identify the predictors contributing most strongly to the RF model while reducing the potential bias associated with impurity-based importance measures. As shown in Fig. 5, the temporal germination variables were the dominant contributors to model performance. Among all predictors, D_{10} exhibited the highest normalized permutation importance (0.156 ± 0.006), followed by D_8 (0.135 ± 0.005), D_9 (0.116 ± 0.004), D_1 (0.091 ± 0.004), D_0 (0.082 ± 0.004), D_7 (0.075 ± 0.004), and D_4 (0.075 ± 0.003). Among the treatment-related variables, MOF concentration was the most influential (0.048 ± 0.003), followed by MOF type (Chemical, 0.038 ± 0.002), NaCl concentration (0.032 ± 0.002), and priming duration (Time, 0.027 ± 0.002). Lower contributions were observed for D_5 (0.041 ± 0.003), D_3 (0.035 ± 0.002), D_6 (0.031 ± 0.002), and D_2 (0.019 ± 0.001), whereas D_{11} exhibited negligible importance (0.000 ± 0.000). Overall, the permutation-based analysis indicates that intermediate and late germination stages contained the greatest predictive information, while the treatment variables provided complementary but comparatively smaller contributions to the model.

3.5. Terahertz time-domain spectroscopy (THz-TDS)

Following the evaluation of temporal germination responses, THz-TDS was employed to characterize treatment-related differences in temporal and spectral dielectric response under MOF-mediated salinity stress environmental conditions. Terahertz Time-Domain Spectroscopy (THz-TDS) is a highly accurate non-destructive technique used to determine the water content in plants. Small changes in a plant's hydration levels lead to immediate and highly sensitive alterations in the amplitude and phase of the transmitted or reflected THz signals. This is primarily because liquid water strongly absorbs terahertz radiation within the frequency range of 0.1–3 THz. The high sensitivity to water is attributed to the collective vibrations of hydrogen bonds; as a result, liquid water acts as an opaque barrier to THz pulses. Consequently, the absorption of THz signals significantly increases with higher water concentration. In addition, increased moisture or free-water content is generally indicated by higher damping in the signal. The THz-TDS analysis showed treatment-dependent differences in the temporal and spectral response of cotton leaf tissues under MOF-mediated salinity stress environmental conditions (Fig. 6a-f). Clear differences in signal

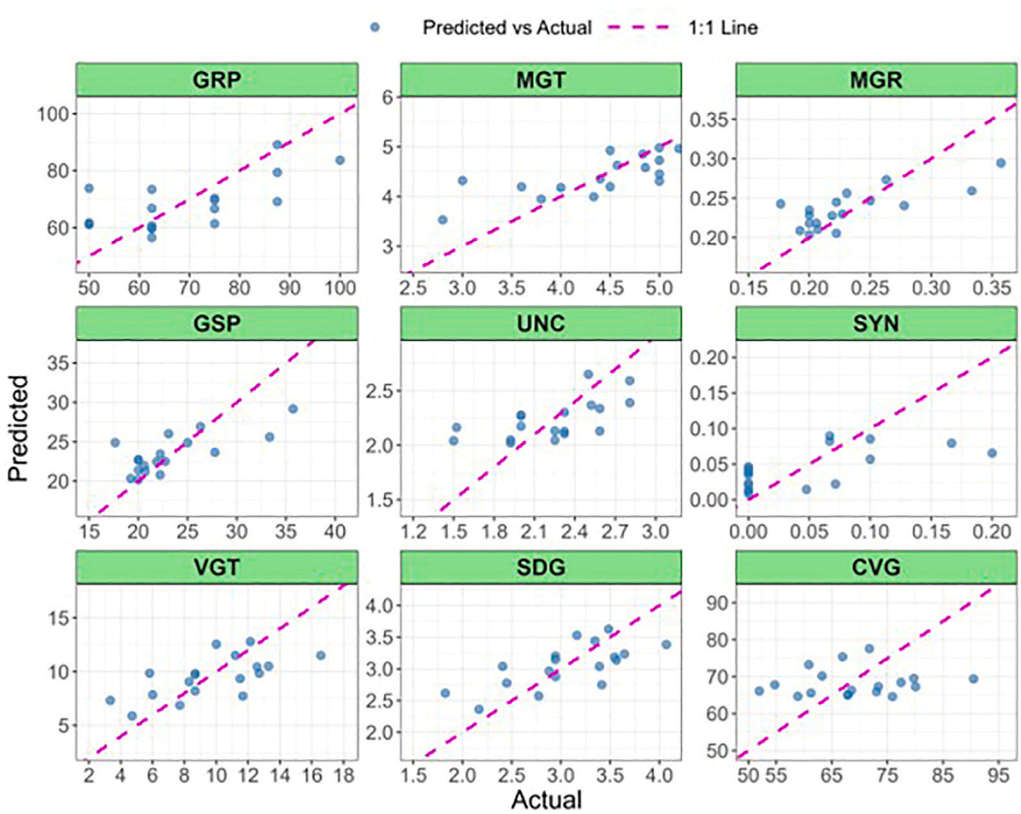

Fig. 4. Experimental and predicted scores of germination indices of cotton (derived from Table 2) using RF-based multi-output regression analysis.

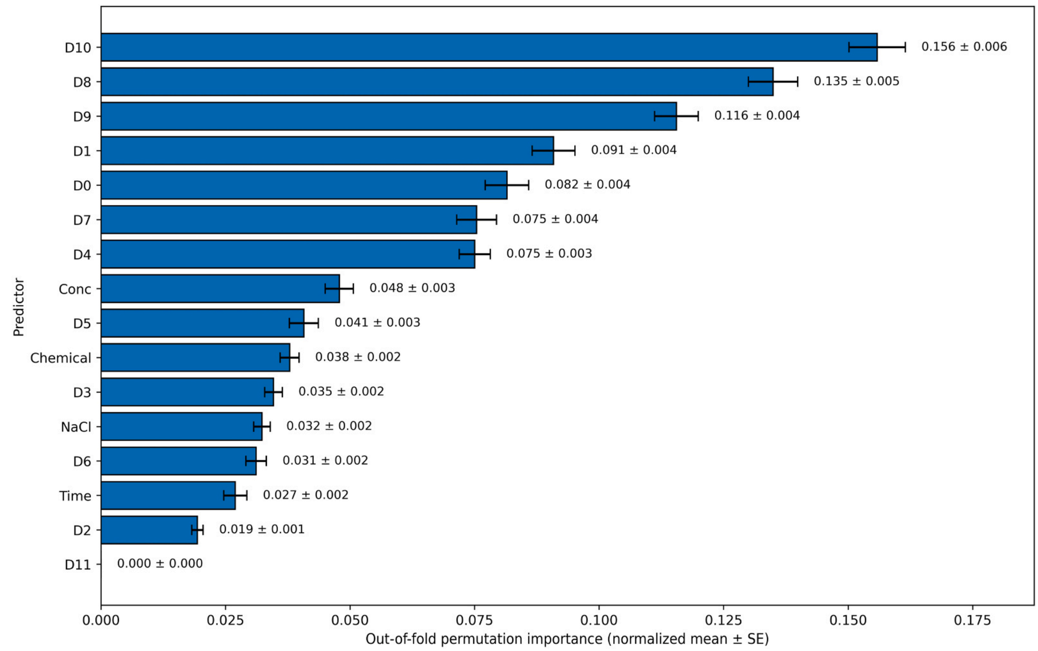

Fig. 5. Permutation feature importance (mean ± SE) of temporal germination variables and treatment-related predictors obtained from the Random Forest model under MOF-mediated salinity stress. Importance values were calculated using held-out observations under the LOOCV framework and normalized across germination traits. values represent mean normalized importance SE across germination outputs and are interpreted as exploratory rankings.

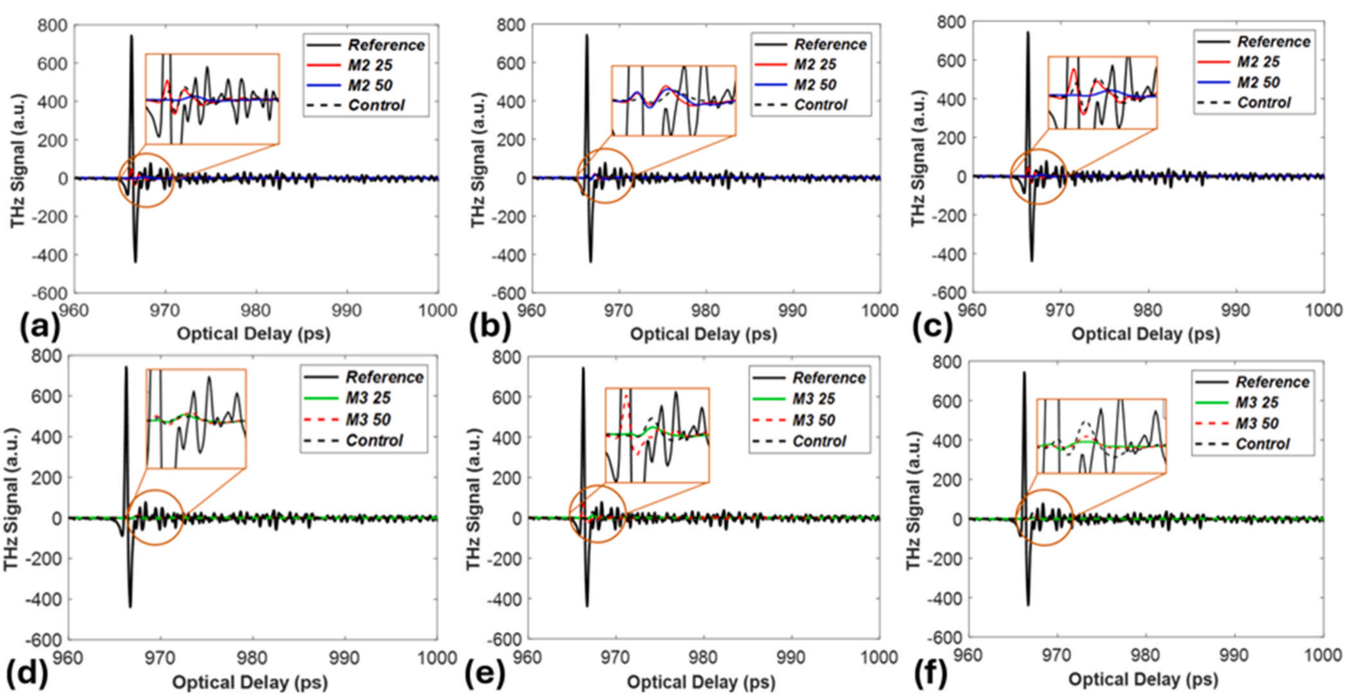

Fig. 6. Time-domain signals of cotton leaf samples (a) Co-MOF for 2 h priming, (b) Co-MOF for 4 h priming, (c) Co-MOF for 8 h priming, (d) Ni-Co-MOF for 2 h priming, (e) Ni-Co-MOF for 4 h priming, and (f) Ni-Co-MOF for 8 h priming with NaCl; Measurements were obtained from independent leaf samples; curves represent descriptive spectral patterns.

attenuation, oscillatory decay, damping characteristics, and absorption coefficient profiles were observed among the evaluated treatment combinations across the 2 h, 4 h, and 8 h priming durations. The transmitted THz time-domain signals displayed considerable differences in amplitude and temporal oscillatory response, suggesting treatment-related modulation of hydration-associated physiological and dielectric properties.

Among the evaluated treatments, Co-MOF−50 exhibited the highest attenuation and smoothest oscillatory decay patterns throughout most observation periods. On the other hand, Co-MOF−25 showed relatively pronounced oscillatory signatures and reduced damping effects, suggesting relatively lower dielectric attenuation and relatively less extensive structural modification during stress exposure. Progressive temporal changes in signal morphology from 2 h to 8 h further displayed dynamic shifts in tissue hydration organization during the experimental period. Clear THz response patterns were also observed within the Ni-

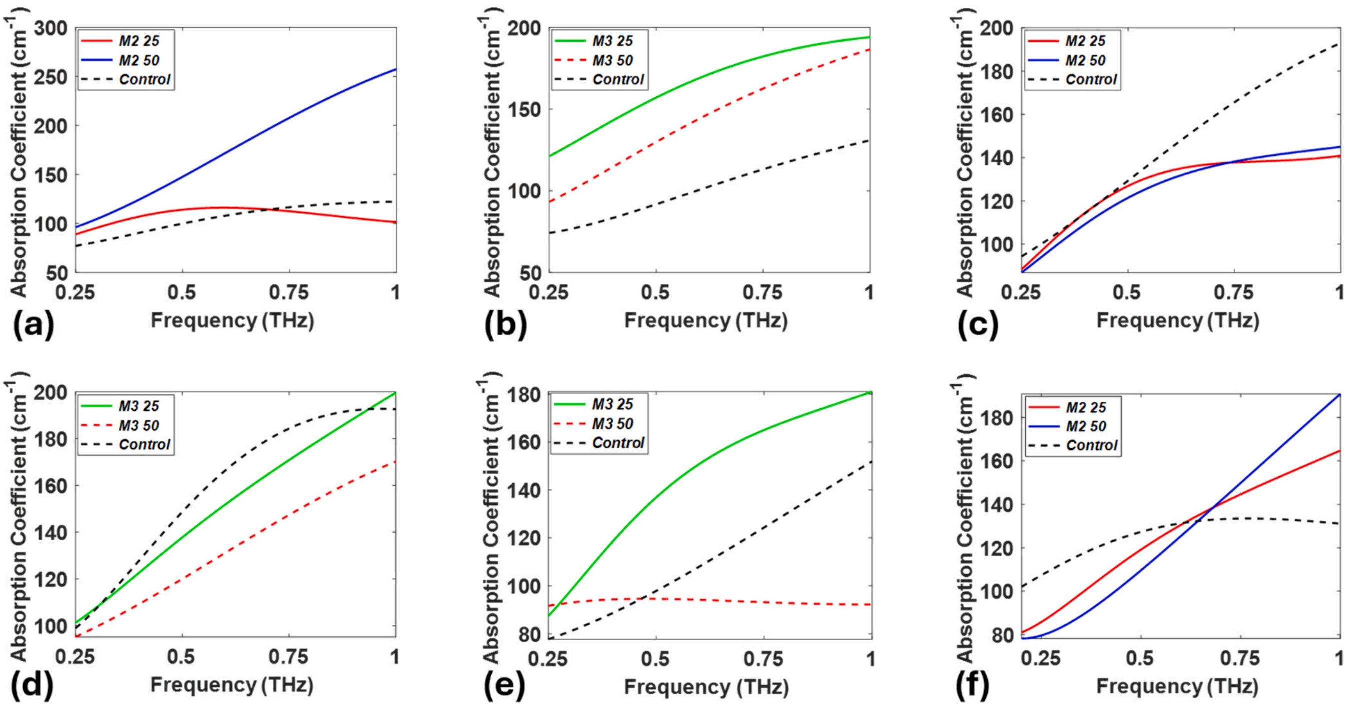

Fig. 7. Absorption Coefficient of cotton leaf samples (a) Co-MOF for 2 h priming, (b) Co-MOF for 4 h priming, (c) Co-MOF for 8 h priming, (d) Ni-Co-MOF for 2 h priming, (e) Ni-Co-MOF for 4 h priming, and (f) Ni-Co-MOF for 8 h priming with NaCl (M2: Co-MOF, M3: Ni-Co-MOF).

Co-MOF treatment system. Compared with Co-MOF-associated treatments, Ni-Co-MOF−25 exhibited relatively stable and homogeneous temporal THz responses across all evaluated priming durations, suggesting a more coordinated dielectric response and relatively stable tissue organization under saline environmental conditions. Conversely, Ni-Co-MOF−50 displayed relatively stronger absorption response accompanied by localized fluctuations and irregular oscillatory features, particularly during later observation periods. Results further showed that 50 mg/L Ni-Co-MOF + 50 mM NaCl exhibited relatively more absorption response compared to 25 mg/L Ni-Co-MOF + 25 mM NaCl and the reference treatment of 100 mM NaCl. Fig. 6a-f presents the absorption coefficient spectra and shows frequency-dependent differences, particularly in the 0.1–1.0 THz region. In general, both MOFs (50 mg/L+50 mM NaCl) yielded higher absorption coefficients across most frequency regions. These elevated THZ absorption responses may indicate treatment-associated changes in tissue hydration dynamics, moisture redistribution, and physiological adaptation under saline environmental conditions. In contrast, relatively reduced absorption with more stable spectral profiles was recorded for both MOFs when used at 25 mg/L + 25 mM NaCl.

4. Discussion

The multi-peak Co-MOF profile agrees with the reported H_2pzdc-based coordination framework, where the carboxylate group bridges adjacent metal centres to form extended periodically ordered networks (Premkumar et al., 2004). The close correspondence between the Co-MOF and Ni-Co-MOF diffraction patterns suggests an isostructural relationship and preservation of the parent crystal topology following Ni incorporation. Similar behavior has been reported for bimetallic Ni-Co-MOF frameworks synthesized using identical organic linkers, where mixed-metal substitution occurred without forming separate crystalline phases (Wu et al., 2023). This structural compatibility is attributed to the comparable ionic radii and coordination behavior of Co^{2+} and Ni^{2+}, which facilitate substitution within the metal nodes while maintaining the framework architecture (Ren et al., 2021). This structural correspondence also agrees with a previously reported pyrazine-containing Ni-Co-MOF [Co/Ni(μ_3-tp)$_2$(μ_2-pyz)$_2$], in which complementary XRD, BET, FT-IR, TGA, SEM, and EDS analyses confirmed the incorporation of both metals within a single crystalline framework (Moradi et al., 2024). The present study showed that MOF-associated salinity treatments substantially influence germination behavior, physiological adaptation patterns, and hydration-associated dielectric responses in cotton under in vitro conditions. The enhanced cumulative germination observed, particularly under the Ni-Co-MOF−50 treatment, suggests that the MOF–NaCl treatment system supported greater germination resilience than the 100 mM NaCl reference condition. Salinity stress commonly suppresses seed germination by reducing water uptake, lowering osmotic potential, inducing Na^+/Cl^- toxicity, disturbing metabolic activity, and promoting oxidative stress (Liang et al., 2018; Atta et al., 2023). Thus, the delayed germination observed under the 100 mM NaCl reference treatment is consistent with the expected inhibitory effects of salt stress on early developmental processes (Manono, 2026). On the other hand, the enhanced germination kinetics under MOF-associated treatments were associated with more favorable temporal germination patterns under saline conditions. This interpretation is also supported by recent plant-related MOF studies showing their potential roles in controlled delivery and improvement of agronomic performance through nutrient delivery, plant-growth modulation, and stress-resilience-related functions (dos Reis et al., 2025; Mahmoud and Abdelhameed, 2025). However, scalable synthesis, formulation stability, and controlled release to ensure consistent exposure while limiting metal accumulation are prerequisites for their application in agriculture (Li et al., 2026)

The clear temporal germination trajectories observed between Co-MOF and Ni-Co-MOF systems suggest that both MOFs have differentially regulated germination dynamics under saline environmental conditions. The Co-MOF system appeared to promote rapid early-stage germination initiation, particularly at the 50 mg/L concentration, indicating its potential role in stimulating early metabolic activation and stress-responsive physiological adjustments. Cobalt-associated materials have previously been linked with enzymatic modulation, osmotic adjustments, and oxidative stress regulation under abiotic stress conditions (Inayat et al., 2024). In contrast, the Ni-Co-MOF system exhibited relatively more stable and sustained germination progression throughout the experimental period, particularly under 50 mg/L treatment. This response reflects a more stable temporal germination pattern under the tested conditions. The presence of both Ni and Co in the MOF structure may have contributed synergistically to improved physiological stabilization and maintained germination synchronization. Since metal-release kinetics, oxidation state, tissue accumulation, and toxicity thresholds were not quantified, the observed effects should be interpreted as a response to the applied MOF formulations rather than as direct evidence of Co- or Ni-Co-specific bioavailability or toxicity. In addition, 4 h priming treatment highlights the importance of optimized exposure time for balancing metabolic activation and stress tolerance in plants (Balasubramaniam et al., 2023; Gohari et al., 2026). Shorter priming durations may provide insufficient physiological stimulation, whereas prolonged exposure can induce stress-associated metabolic disorders (Paparella et al., 2015; Janah et al., 2025). The progressive increase in cumulative germination at late stages further suggests dynamic physiological adaptation and recovery processes during prolonged salinity stress exposure.

The RF-based multi-output regression analysis (Altaf et al., 2026) demonstrated variable predictive learnability among germination-related traits under MOF-mediated salinity stress conditions. Traits such as MGR, GSP, SDG, and GPR showed relatively better but modeate predictive performance, indicating that RF captured part of their nonlinear variation. RF models are increasingly recognized for modeling complex biological datasets because of their ability to capture nonlinear interactions and multidimensional physiological variability (Hoffman et al., 2021; Altaf et al., 2026). In contrast, SYN and CVG showed poor predictive performance, especially, extreme relative errors (SYN) and negative R^2 scores (CVG) highlight trait-specific limitations and define the model's applicability. These findings demonstrate the usefulness of explainable ML approaches for interpreting germination-associated physiological responses and stress adaptation under saline conditions (Ercan et al., 2024; Yan et al., 2025; Aasim et al., 2026).

The use of permutation importance, which evaluates predictor relevance by measuring the reduction in predictive performance after random permutation of individual variables, provides a more robust assessment than impurity-based importance measures and strengthens the biological interpretation of the identified key germination stages. Permutation feature importance (Huang, 2025) analysis revealed that the temporal germination observations were the dominant contributors to the RF model, particularly for D_{10}, $D_{8,}$ and $D_{9,}$ which exhibited the highest normalized importance values, followed by D_1, D_0, D_7, and D_4. These findings suggest that intermediate and late germination stages contain the greatest amount of predictive information, likely reflecting the cumulative effects of MOF treatment and salinity stress on germination dynamics. Among the treatment-related variables, MOF concentration, MOF type, NaCl concentration, and priming duration also contributed to model performance, although their influence was comparatively smaller than that of the temporal germination observations. These findings further suggest the temporal coordination of the germination process under MOF-mediated salinity stress conditions, confirming the previous findings (Khanna et al., 2019; Tietze et al., 2025). The strong influence of temporal germination stages further highlights the importance of germination kinetics and developmental coordination in ML-assisted interpretation of plant stress under saline environments (Quyoom et al., 2026; Yang et al., 2026). Although RF model identified meaningful nonlinear relationships among the germination traits, using LOOCV that is well suited for limited datasets. Nevertheless, the absence of an independent external validation dataset remains a limitation; the proposed framework should be considered as an exploratory analytical approach.

The results of THz-TDS analysis showed considerable treatment-dependent differences in dielectric tissue response and hydration-associated physiological responses. The stronger attenuation and elevated absorption response observed under the Co-MOF−50 mg/L and Ni-Co-MOF−50 treatments indicate enhanced interaction between THz radiation and hydration-associated physiological and dielectric components within the leaf tissues. The stronger damping response observed in this treatment is consistent with greater THz absorption within the leaf tissues, which may reflect combined differences in water status, tissue thickness, structural organization, and chemical composition. THz signals are highly sensitive to tissue water content, hydrogen-bond dynamics, and cellular tissue hydration organization and structural stability, making THz-TDS a powerful tool for monitoring physiological stress responses in plants (Castro-Camus et al., 2025; You et al., 2025). In the present study, the elevated damping response observed particularly under Co-MOF−50 mg/L suggests considerable modification of hydration-associated dielectric properties during salinity stress exposure. The relatively stable and homogeneous THz signatures observed in Ni-Co-MOF−25 showed a relatively uniform treatment-associated dielectric response under saline conditions.Similar stabilization of THz spectral response has been linked with improved tissue water balance and structural integrity under abiotic stress conditions (Castro-Camus et al., 2025). The observed differences in absorption profiles and oscillatory behavior likely reflect treatment-associated modulation of tissue hydration and structural organization within the leaf tissues (Taiber et al., 2025). In addition, recent advances in plant THz phenotyping have highlighted the potential of THz-TDS for non-destructive characterization of physiological stress responses, early stress detection, and monitoring of hydration-associated changes in plant tissues under environmental stress conditions (Alibeigloo et al., 2025; Gao et al., 2025). The treatment-resolved spectral fingerprints established as a basis for future paired analysis linking THz features with germination and physiological measurements collected from the same experimental units in future studies.

The progressive temporal shifts observed in THz signal morphology from 2 h to 8 h further suggest dynamic physiological adjustment processes involving moisture redistribution, structural dielectric reorganization, and stress-associated tissue adaptation (Yin et al., 2026). Similar temporal THz response patterns have been associated with dehydration dynamics and physiological adaptation in plant tissues under abiotic stress conditions (Alibeigloo et al., 2025; You et al., 2025). Localized fluctuations observed in Ni-Co-MOF−50 may reflect heterogeneous redistribution of hydration-associated structural components during prolonged stress exposure. The absorption coefficient spectra further revealed frequency-dependent differences among the evaluated treatments, confirming substantial differences in THz interaction responses within the cotton leaf tissues. Frequency-dependent THz absorption is strongly influenced by tissue water status and hydrogen-bond dynamics within biological tissues (Castro-Camus et al., 2025). THz-TDS findings demonstrate that terahertz spectroscopy effectively captured treatment-specific physiological adaptation patterns under MOF-mediated salinity stress environmental conditions and further support its potential as a non-destructive phenotyping platform for monitoring stress-associated physiological responses in plants (Alibeigloo et al., 2025; Taiber et al., 2025; You et al., 2025). The distinct-hydration-sensitive dielectric signatures detected by THz-TDS provide a basis for future integration with direct measurements of water status, photosynthetic performance, oxidative responses, and membrane stability to further define their physiological significance (Yu-Hao et al., 2025; Yin et al., 2026).

5. Conclusion

MOF-associated salinity treatments substantially influenced germination kinetics, temporal coordination of development, and dielectric tissue responses in cotton under in vitro saline conditions. Among the evaluated treatment combinations, Ni-Co-MOF−50 exhibited the highest cumulative germination performance, whereas the relatively stable THz signatures observed in Ni-Co-MOF−25 suggested enhanced physiological stability and coordinated dielectric regulation during stress exposure. On the other hand, the 100 mM NaCl reference treatment displayed a delayed germination response and relatively reduced physiological performance, confirming the inhibitory effects of elevated salinity on germination-associated processes. The observed treatment-dependent differences in cumulative germination patterns, temporal synchronization behavior, and THz absorption profiles demonstrate an association between the applied MOF formulations and early germination and dielectric responses under salinity. The RF framework successfully identified trait-dependent nonlinear patterns, with comparatively better performance for MGR, GSP, SDG, and GRP, whereas SYN and CVG were not reliably predicted. Additionally, feature importance analysis identified intermediate germination stages as key determinants of predictive performance, highlighting the physiological significance of temporal germination dynamics during stress adaptation. THz-TDS analysis further revealed distinct treatment-dependent variations in dielectric response and hydration-associated structural organization within cotton leaf tissues. The integration of temporal germination profiling, explainable machine learning, and THz-TDS provided an integrated framework for characterizing MOF-mediated salinity responses in cotton. The combined analytical strategy highlights the potential of integrating next-generation spectroscopic and interpretable AI approaches for non-destructive plant stress phenotyping under saline environments. Future integration of physiological and omics studies will help to define the pathways underlying the observed MOF-associated responses.

CRediT authorship contribution statement

Kholoud Elmabruk: Writing – review & editing, Writing – original draft, Formal analysis. **Salma Naimatullah Soomro:** Writing – original draft, Methodology. **Sabeen Rehman Soomro:** Writing – original draft, Methodology. **Tülay Aksoy:** Writing – original draft, Methodology. **Kağan Murat Pürlü:** Methodology. **Seyid Amjad Ali:** Writing – original draft, Resources, Methodology. **Emre Biçer:** Writing – original draft, Methodology. **Sabit Horoz:** Writing – review & editing, Formal analysis. **Waqas Liaqat:** Writing – review & editing, Formal analysis. **Kağan Kökten:** Writing – review & editing, Resources. **Muhammad Aasim:** Writing – review & editing, Writing – original draft, Supervision, Conceptualization. **Muhammad Tanveer Altaf:** Writing – review & editing, Writing – original draft, Funding acquisition.

Funding

This study was supported by the Recep Tayyip Erdoğan University Development Foundation (Grant number: 02026008014568).

Declaration of Competing Interest

The authors declare that they have no known competing financial interests or personal relationships that could have appeared to influence the work reported in this paper.

Data availability

shared in the article

References

Aasim, M., Aydin, E.S., Korkut, I., Ergan, B.T., Say, A., Soomro, S.N., Soomro, S.R., Ali, S. A., Ercişli, S., Katırcı, R., 2026. Machine learning and design of experiment for enhanced biomass using N2 and CO2-enriched biochar at different pyrolysis temperatures. Biomass Bioenergy 208, 108803.
Aasim, M., Yıldırım, B., Say, A., Ali, S.A., Aytaç, S., Nadeem, M.A., 2024. Artificial intelligence models for validating and predicting the impact of chemical priming of hydrogen peroxide (H2O2) and light emitting diodes on in vitro grown industrial hemp (Cannabis sativa L.). Plant. Mol. Biol. 114, 33.
Alibeigloo P., Preuss C., Mutlu E., Sheikh F., Zantah Y., Prokscha A., Watermann J., Abts J., Kress R., Clochiatti S. (2025) Plant Water Content Monitoring Using Miniaturized THz RTD Oscillators and Detectors. 1–5.
Altaf, M.T., Aasim, M., Mustafa, Z., Ali, S.A., 2026. Chitosan nanoparticles induced germination and auxin-related gene regulations in cotton (Gossypium hirsutum L.) using random forest-based multi-output regression analysis. Ind. Crops Prod. 243, 123035.
Atta, K., Mondal, S., Gorai, S., Singh, A.P., Kumari, A., Ghosh, T., Roy, A., Hembram, S., Gaikwad, D.J., Mondal, S., 2023. Impacts of salinity stress on crop plants: improving salt tolerance through genetic and molecular dissection. Front. Plant. Sci. 14, 1241736.
Bakhsh, A., Anayol, E., Özcan, S.F., Hussain, T., Aasim, M., Khawar, K.M., Özcan, S., 2015. An insight into cotton genetic engineering (Gossypium hirsutum L.): current endeavors and prospects. Acta Physiol. Plant. 37.
Balasubramaniam, T., Shen, G., Esmaeili, N., Zhang, H., 2023. Plants' response mechanisms to salinity stress. Plants 12, 2253.
Borchani, H., Varando, G., Bielza, C., Larranaga, P., 2015. A survey on multi-output regression. Wiley Interdiscip. Rev. Data Min. Knowl. Discov. 5, 216–233.
Breiman, L., 2001. Random forests. Mach. Learn. 45, 5–32.
Castro-Camus, E., Singh, A.K., Perez-Lopez, A.V., Morales-Hernandez, J.A., Simpson, J., Villanueva-Rodriguez, S.J., Ortiz-Martinez, M., 2025. Terahertz spectroscopy and imaging as a tool to unlock physiological and molecular mechanisms for drought resistance of agaves. Appl. Opt. 64, 2057–2062.
Elkelish, A., Alqudah, A.M., Alhudhaibi, A.M., Thabet, S.G., 2026. Framework-primed trehalose: fast-tracking abiotic stress memory. Plant. Cell. Rep. 45, 15.
Ercan, U., Kabas, O., Moiceanu, G., 2024. Prediction of leaf break resistance of green and dry alfalfa leaves by machine learning methods. Appl. Sci. 14, 1638.
Gao, H., Liu, Y., Li, G., Liu, H., Shang, Y., Niu, Y., 2025. Diagnosis of low-light stress in lettuce using a quad-resonance peak terahertz metamaterial sensor. Infrared Phys. Technol., 106280
Ginzburg, D.N., Cox, J.A., Rhee, S.Y., 2024. Non-destructive, whole-plant phenotyping reveals dynamic changes in water use efficiency, photosynthesis, and rhizosphere acidification of sorghum accessions under osmotic stress. Plant. Direct 8, e571.
Gohari, G., Spanos, A., Ioannou, A., Efstathiou, I., Panahirad, S., Kolbert, Z., Fotopoulos, V., 2026. Seed priming approaches for climate-resilient agriculture. J. Exp. Bot. 77, 2013–2026.
Hoffman K., Sung J.Y., Zazzera A. (2021) Multi-output random forest regression to emulate the earliest stages of planet formation. 1–6.
Huang, P., 2025. Residual permutation tests for feature importance in machine learning. Br. J. Math. Stat. Psychol.
Inayat, H., Mehmood, H., Danish, S., Alharbi, S.A., Ansari, M.J., Datta, R., 2024. Impact of cobalt and proline foliar application for alleviation of salinity stress in radish. BMC Plant. Biol. 24, 287.
Janah, I., Elhasnaoui, A., Laouane, R.Ben, Ait-El-Mokhtar, M., Anli, M., 2025. Exploring seed priming as a strategy for enhancing abiotic stress tolerance in cereal crops. Stresses 5, 39.
Khanna, R., Schmid, L., Walter, A., Nieto, J., Siegwart, R., Liebisch, F., 2019. A spatio temporal spectral framework for plant stress phenotyping. Plant. Methods 15, 13.
Li, A., Li, C., Zheng, Z., Zhu, L., Wang, Z., Xie, D., 2026. A cellulose nanofiber assembled nanoporous membrane with exceptional dye desalination. Desalination, 119910.
Liang, W., Ma, X., Wan, P., Liu, L., 2018. Plant salt-tolerance mechanism: a review. Biochem. Biophys. Res. Commun. 495, 286–291.
Liu, Y., Liu, A., Qin, J., Yang, Y., 2026. Metal-organic frameworks for alleviating environmental stress in crops. Chem. Rec., e202500270
Mahmoud, N.E., Abdelhameed, R.M., 2025. Influence of different metal-organic frameworks on agronomic traits of faba bean plants. BMC Plant. Biol. 25, 1485.
Manono, B.O., 2026. Effects of salinity on seed germination: mechanisms, impacts, and mitigation strategies. Seeds 5.
Masood, H.A., Ahmed, T., Zahid, M.K., Noman, M., Yousaf, M.A., Ali, H.M., Li, B., Han, S., 2025. Metal–organic frameworks as versatile platforms for sustainable crop disease management: a comprehensive review of mechanisms and applications. Environ. Sci. Nano 12, 3425–3441.
Moradi, E., Salehi, M.M., Maleki, A., 2024. Highly stable mesoporous Co/Ni mixed metal-organic framework [Co/Ni (μ3-tp) 2 (μ2-pyz) 2] for Co (II) heavy metal ions (HMIs) remediation. Heliyon 10.
Muhammad, A., Khan, Z.U., Khan, J., Mashori, A.S., Ali, A., Jabeen, N., Han, Z., Li, F., 2025. A comprehensive review of crop stress detection: destructive, non-destructive, and ML-based approaches. Front. Plant. Sci. 16, 1638675.
Muthalagu, S., Natarajan, S., 2025. Agricultural innovation through metal–organic frameworks: exploring fundamentals and applications - recent advances and future prospects. Sci. Total. Environ. 998, 180225.
Nie, Y., Li, D., Peng, Y., Wang, S., Hu, S., Liu, M., Ding, J., Zhou, W., 2020. Metal organic framework coated MnO2 nanosheets delivering doxorubicin and self-activated DNAzyme for chemo-gene combinatorial treatment of cancer. Int. J. Pharm. 585, 119513.
Okumuş, O., Say, A., Eren, B., Demirel, F., Uzun, S., Yaman, M., Aydın, A., 2024. Using machine learning algorithms to investigate the impact of temperature treatment and salt stress on four forage peas (Pisum sativum var. arvense L.). Horticulturae 10, 656.
Özdemir, S., Giray, G., Aksoy, T., Biçer, E., Gonca, S., Köşe Kaya, K., Orak, C., Horoz, S., 2026. Multifunctional activities of Cu-, Ni-, and Co-metal–organic frameworks: structural, photocatalytic, and biological insights. Polyhedron 289, 118016.
Paparella, S., Araújo, S.S., Rossi, G., Wijayasinghe, M., Carbonera, D., Balestrazzi, A., 2015. Seed priming: state of the art and new perspectives. Plant. Cell. Rep. 34, 1281–1293.
Premkumar, T., Govindarajan, S., Starosta, W., Leciejewicz, J., 2004. Pyrazine-2, 3-dicarboxylic acid. Struct. Rep. 60, o1305–o1306.

Purlu, K.M., Dalgac, S., Isik, E., Yildiz, B.K., Elmabruk, K., 2026. Strontium oxide-doped alumina-based functional ceramics: microstructure, dielelectric properties, and suitablility for 5G/6G and millimeter-wave applications. J. Mater. Sci. Mater. Electron. 37, 322.
Quyoom, B., Wani, A.A., Lone, A.A., Dar, Z.A., Mir, B.A., Peer, L.A., 2026. A maize-centric framework for explainable artificial intelligence in decoding drought tolerance mechanisms. Discov. Plants 3, 18.
dos Reis, R.A., Fernández-Baldo, M.A., Nunes, R.S., Seabra, A.B., 2025. Metal-organic frameworks: An overview of a possible solution for modern agriculture. Microporous Mesoporous Mater. 391, 113609.
Ren, F., Ji, Y., Chen, F., Qian, Y., Tian, J., Wang, J., 2021. Flower-like bimetal Ni/Co-based metal–organic-framework materials with adjustable components toward high performance solid-state supercapacitors. Mater. Chem. Front. 5, 7333–7342.
Rojas, S., Rodríguez-Diéguez, A., Horcajada, P., 2022. Metal–organic frameworks in agriculture. ACS Appl. Mater. Interfaces 14, 16983–17007.
Saini, Y., Somani, V., Khatri, N., 2026. Critical analysis of advanced machine learning and deep learning models for crop disease detection: challenges, innovations, and future directions. Frankl. Open. 15, 100584.
Taiber, J., Helminiak, J., Hernandez-Cardoso, G.G., Mach, C., Jäckel, A., Naranjo-Montoya, O.A., Castro-Camus, E., Ache, P., Hedrich, R., Koch, M., 2025. The dynamics of stomatal closure of Arabidopsis thaliana determined by terahertz spectroscopy and a water transport model. Sci. Rep. 15, 32675.
Tietze, H., Abdelhakim, L., Pleskačová, B., Kurtz-Sohn, A., Fridman, E., Nikoloski, Z., Panzarová, K., 2025. Prediction of harvest-related traits in barley using high-throughput phenotyping data and machine learning. Front. Plant. Sci. 16, 2025.
Tsoumakas G., Vlahavas I. (2007) Random k-labelsets: An ensemble method for multilabel classification. 406–417.
Wang, Y., Cheng, Z., Wang, Z., 2024. Multi-Output Bayesian Support Vector Regression Considering Dependent Outputs. Mathematics 12, 2923.
Wu, L., Shao, H., Li, J., Chen, C., Hu, N., Yang, B., Weng, H., Xiang, L., Ye, D., 2024. Noninvasive abiotic stress phenotyping of vascular plant in each vegetative organ view. Plant. Phenom. 6, 180.
Wu, D., Zhang, Q., Zhang, M., Yang, J., Yang, J., Hu, T., Wang, X.-Q., 2023. Self-assembled cobalt–nickel bimetallic-organic framework materials with high supercapacitor performance. Cryst. Growth Des. 23, 3978–3987.
Yan, J., Wu, H., Diao, Z., Miao, Y., Zhang, B., Zhao, C., 2025. Recent developments and applications of crop disease detection, prediction, and early warning: a review. Engineering. https://doi.org/10.1016/j.eng.2025.10.032.
Yang, R., Zhu, H., Xu, F., Guo, W., Lu, M., Chen, D., Jiang, X., Han, Z., Zhao, C., 2026. Deep learning and XAI-enabled prediction of maize seed vigor phenotypes and physiological trait with spectral feature association analysis. Comput. Electron. Agric. 240, 111216.
Yin, H., Bista, P., Ghimire, R., Yang, H., Carroll, K.C., 2026. Unraveling soil moisture dynamics with dual-scale interpretable machine learning: cover cropping and irrigation insights in semi-arid agriculture. Vadose Zo J. 25, e70077.
You, X., Pagay, V., Withayachumnankul, W., 2025. Non-contact monitoring of plant leaf water status using terahertz waves. J. Infrared Millim. Terahertz Waves 46, 53.
Yousef, F., Shafique, F., Ali, Q., Malik, A., 2020. Effects of salt stress on the growth traits of chickpea (Cicer arietinum L.) and pea (Pisum sativum L.) seedlings. Biol. Clin. Sci. Res. J. 2020.
Yu-Hao, D., Chun, C., Ping-Ping, W., Chun, W., Xiong, F., 2025. Sugarcane extract enhances stress resilience and longevity in Caenorhabditis elegans: NMR structural elucidation and transcriptomic mechanisms. Food Res. Int., 117863
Zarbakhsh, S., Fakhrzad, F., Rajkovic, D., Niedbała, G., Piekutowska, M., 2025. Approaches and challenges in machine learning for monitoring agricultural products and predicting plant physiological responses to biotic and abiotic stresses. Curr. Plant. Biol. 43, 100535.
Zhu, P., Li, R., Lu, A., 2024. Electrode impedance modeling based on XGboost algorithm for analyzing the antioxidant properties of juice. J. Food Meas. Charact. 18, 5031–5042.